1 # Structure-guided optimization of light-activated

2 # chimeric G-protein coupled receptors

3

4

5

6

7

8

9 Alexandra-Madelaine Tichy[a,b], Wang Lok So[a,b], Elliot J. Gerrard[a,b,c] and Harald Janovjak[a,b,*]

10

11 [a] Australian Regenerative Medicine Institute (ARMI), Faculty of Medicine, Nursing and Health

12 Sciences, Monash University, 3800 Clayton/Melbourne, Australia.

13 [b] European Molecular Biology Laboratory Australia (EMBL Australia), Monash University, 3800

14 Clayton/Melbourne, Australia.

15 [c] Commonwealth Scientific and Industrial Research Organisation, Synthetic Biology Future

16 Science Platform, Monash University, 3800 Clayton/Melbourne, Australia.

17

18

19

20

21

22

23

24

25

26

27

28

29

32

33

34 * To whom correspondence should be addressed.

35 Email: harald.janovjak@monash.edu

36 +61 3 99029612

ABSTRACT

G-protein coupled receptors (GPCRs) are the largest human receptor family and involved in virtually every physiological process. One hallmark of GPCR function is the specific coupling of activated receptors to selected downstream signaling pathways. The ability to tune this coupling would permit the development of receptors with new capabilities. GPCRs and G-proteins have been recently resolved structurally at high resolution, but this information was in only very few cases harnessed for a rational engineering of these protein complexes. Here, we demonstrate the structure-guided optimization of coupling in chimeric light-activated GPCRs (OptoXRs). Our hypothesis was that the incorporation of structural GPCR-Gα contacts will lead to improved receptor activity. We first evaluated structure-based alignments as complements to existing sequence-based methods for generation of chimeric receptors. We then show in a prototypical light-activated β_2AR that inclusion of α-helical residues forming structural contacts to Gα resulted in receptors with 7- to 20-fold increased function compared to other design strategies. In turn, elimination of GPCR-Gα contacts diminished function. Finally, the efficient receptor design served as a platform for the optimization of a further light-activated receptor and spectral tuning of the photoreceptor core domain. Our work exemplifies how increased OptoXR potency and new functionalities can be achieved through structure-based design towards targeted inputs into cells and cellular networks.

INTRODUCTION

G-protein coupled receptors (GPCRs) comprise the largest family of membrane receptors in the human genome. They are expressed broadly and regulate key biological processes, ranging from organism development to metabolism and brain function[1,2]. In line with their abundance and physiological importance, GPCRs are also exceptional therapeutic targets with ~30% of all prescription drugs acting on members of this receptor superfamily[3,4].

Canonical signaling downstream of GPCRs is mediated through coupling to heterotrimeric G-proteins, which are often classified into four main groups according to their Gα subunits (the $G\alpha_s$, $G\alpha_{i/o}$, $G\alpha_q$ and $G\alpha_{12/13}$ groups). Gα subunits principally act on adenylyl cyclase to increase ($G\alpha_s$) or decrease ($G\alpha_{i/o}$) cAMP levels, on phospholipase C (PLC) to alter Ca^{2+} signaling ($G\alpha_q$) or on Rho GTPases ($G\alpha_{12/13}$) to modulate motor proteins and the cytoskeleton (**Fig. 1a**). In addition, associated Gβ and Gγ subunits activate ion channels and a wide range of enzymes upon dissociation of the trimeric complex. In humans, at least 16 Gα subunits, 6 Gβ subunits and 13 Gγ subunits have been identified, which can assemble in a multitude of combinations leading to functionally-distinct outcomes[5-7]. GPCRs can also signal *via* β-arrestin scaffolding proteins ultimately to diverse signaling pathways (**Fig. 1a**). Importantly, the expression of multiple GPCRs and G-proteins in many cell types results in combinatorial complexity and dictates that specific GPCR-G-protein interactions guide signaling outcomes[5,8].

Consequences of GPCR signaling are most commonly studied using pharmacological (e.g., agonists, antagonists or allosteric modulators) or genetic methods (e.g., receptor overexpression or knock-out) in cells and animals. As a complement, approaches have been developed to (in)activate GPCR signaling on shorter time scales and finer spatial scales than those dictated by drug diffusion or pharmacokinetics and those associated with genetic alterations[9,10]. One such approach are light-activated GPCRs, which are either repurposed from naturally light-sensing mammalian tissues[11-13] or from invertebrates and fish[14-17], or are engineered as chimeric GPCRs (termed OptoXRs)[18,19]. Albeit of different sources, these light-activated GPCRs all permit spatio-temporal activation of signaling pathways by light in the emerging field of optogenetics[20,21].

The purpose-built OptoXRs take advantage of conserved structure-function relationships by substituting the downstream coupling domains of a light-gated GPCR, such as the mammalian dim light sensor rhodopsin (rho), with those of a naturally ligand-gated target GPCR (**Fig. 1b**)[18,19]. The desired engineering outcome is that the chimeric GPCR can be activated by light but retains the signaling properties of the target receptor. OptoXRs have been expressed in neuronal and non-neuronal cell types *ex vivo* and *in vivo* using viral delivery or in transgenic animals and activated with light from a variety of sources[22-24]. Light control was often achieved *in vivo* without supplementation of the *cis*-isoform retinal cofactor[18,25,26],

92   but supplementation protocols have also been developed[22]. The OptoXR methodology has
93   been applied to a number of target GPCRs by us and others (see **Supplementary Table S1**
94   for a -to our best knowledge- comprehensive list of OptoXRs). Notably, the design principle
95   underlying most published receptors (see column "Domain Boundaries" in **Supplementary**
96   **Table S1**) was derived from a pioneering study[19] that employed a trial-and-error screening
97   strategy (i.e., various receptor residues and receptor domains were swapped and the
98   emerging receptors tested functionally). This original and more recent trial-and-error designs
99   have put forward the notion that intracellular loops (ICLs) are dominant determinants of
100 function in OptoXRs[19,27], but this has never been tested systematically[9]. The increasing
101 application of chimeric and natural light-activated GPCRs not only as basic research tools but
102 even potential future treatment strategies[23,28,29] calls for attempts to rationally engineer
103 OptoXRs to, e.g., improve or diversify their function.

104   In the past decade, the structural information available for GPCRs has increased
105 dramatically to encompass more than 600 high-resolution structures for more than 150 unique
106 receptors[1,30]. Detailed analyses of these structures have provided insights into GPCR
107 structure-function relationships, such as the universal heptahelical transmembrane (TM)
108 domain, the translation and rotation of specific TM α-helices upon receptor activation or the
109 switch-like behavior of conserved residue networks[31-35]. Following from early successes using
110 X-ray crystallography[36], it was the advent of cryo-electron microscopy (cryo-EM) that revealed
111 a number of active state and G-protein bound structures for members of several major GPCR
112 classes[37-39]. Albeit structures of GPCR-Gα complexes allow identifying key molecular
113 interactions between GPCRs and their downstream transducers[5,36,40], this knowledge has
114 been in only very few cases harnessed for the development of receptors with rationally-
115 designed downstream functions[9,41]. Specifically, orthogonal Gα subunits[42] or GPCRs with
116 promiscuous downstream coupling[43] were designed using modelling, molecular dynamics
117 simulations and *in silico*/experimental mutagenesis. It remains to be further explored to what
118 extent GPCR function can be redesigned using strategies that build on the identification of
119 GPCR-G-protein contacts. Such strategies may complement seminal work in which
120 downstream coupling in wildtype (WT) and chimeric GPCRs was altered through residue
121 substitutions that were derived from functional screens or biochemical assays[26,44,45].

122   Here, we optimized OptoXR function by harnessing high-resolution GPCR-Gα
123 structures. Besides potential future applications in optogenetics, we chose OptoXRs as a
124 model system because an efficient switch in coupling, e.g. from the native G$\alpha_{i/o}$ preference of
125 rho to a different Gα group of the target receptor, is required for the faithful function of these
126 chimeric receptors. We first explored if atomic structure superpositions are a required
127 complement to sequence alignments for determination of functional domain boundaries. We
128 then developed rational structure analysis and receptor design strategies. Focusing on

129 GPCRs in complex with their restive Gα subunits, we showed that inclusion of TM α-helical

130 residues that form contacts to Gα greatly improved functionality of a light-activated β2AR

131 receptor. Finally, we demonstrated optimization of a second receptor and tuning of spectral

132 properties. Collectively, the major advance of this work is a demonstration of structure-guided

133 reengineering of GPCR-Gα coupling yielding improved and diversified OptoXRs.

134

135

136 **METHODS**

137 **Vectors and constructs**

138 OptoXR genes were designed as described in the main text and ordered as synthetic genes

139 (gBlocks, Integrated DNA Technologies). Protein and nucleotide sequences of all engineered

140 receptors can be found in **Supplementary Table S3** and **Supplementary Table S4**,

141 respectively. Genes were amplified in polymerase chain reactions (PCRs) using

142 oligonucleotides with XhoI and KpnI restriction site overhangs and digested with the respective

143 enzymes (NEB). pcDNA3.1 (Thermo Fisher Scientific) was digested with the same enzymes

144 and ligated with the amplified receptors using T4 DNA ligase (Promega).

145 For β-arrestin recruitment assays, receptors were tagged with Rluc8[46]. Receptor genes

146 were amplified without a stop codon using oligonucleotides with BamHI and XhoI restriction

147 site overhangs and digested with the respective enzymes. A vector containing Rluc8 (a kind

148 gift of P. Sexton, Monash University) was digested with the same enzymes. Receptor genes

149 were ligated into the vector N-terminally of Rluc8 using T4 DNA ligase.

150 Opto-β2AR and Opto-A2AR vectors were in the same backbone and described in a

151 previous publication[47]. The Opto-β2AR gene encodes for a protein that is identical to those

152 published previously[18,19]. β2AR in pcDNA3 was a gift of Robert Lefkowitz (Addgene plasmid

153 #14697)[48]. JellyOp in pcDNA3.1 was a kind gift of Robert Lucas[16].

154 Single and double residue substitutions were introduced in Opto-β2AR-2.0 using

155 overlapping oligonucleotides (designed in PrimerX (https://www.bioinformatics.org/primerx/)

156 using the QuikChange option) and circular PCRs with a high-fidelity polymerase (Q5, NEB)

157 followed by digestion with DpnI restriction enzyme (NEB).

158 All genes were verified using Sanger sequencing (MicroMon, Monash University).

159

160 **Cell culture**

161 HEK293 cells (Thermo Fisher Scientific; further authenticated by assessing cell morphology

162 and growth rate) were cultured in mycoplasma-free Dulbecco's modified Eagle medium

163 (DMEM, Gibco) in a humidified incubator with 5% CO_2 atmosphere at 37°C. Medium was

164 supplemented with 10% FBS, 100 U/ml penicillin and 0.1 mg/ml streptomycin (Gibco).

165 HEK293 cells were reverse transfected using poly(ethyleneimine) (linear, 20 kDA;

166   Polysciences)[49]. Culture medium was changed 6 h after transfection and supplemented with

167   10 µM 9-*cis*-retinal (Sigma) for experiments with light-activated receptors.

168

Real-time cAMP measurements

170   The real-time cAMP assay employed the GloSensor-22F reporter cloned into pcDNA3.1 as

171   described previously[47]. HEK293 cells were seeded at a density of 5 x 10^4 cells/well in white

172   96-well plates and transfected with receptor and reporter at a ratio of 1:1. HEK293 cells

173   endogenously express β_2AR and were mock transfected with empty vector backbone for β_2AR

174   conditions. The next day, culture medium was changed to Leibovitz's L15 (Gibco) starve

175   medium (0.5% FBS, 100 U/ml penicillin and 0.1 mg/ml streptomycin) supplemented with 2 mM

176   D-luciferin (Cayman Chemicals) and 10 µM 9-*cis*-retinal in experiments with light-activated

177   receptors. Cells were incubated for 60 min at room temperature (RT). Luminescence was

178   measured in a microplate reader (Omega, BMG Labtech). Baseline luminescence values were

179   recorded for 8 cycles (90 s/cycle) before stimulation. Cells were stimulated with light or ligand

180   as described in the main text and figure captions. For PTX experiments, cells were incubated

181   with 10 µM PTX (List Labs) overnight (o/n) at 37°C. Light stimulation employed the Xenon

182   white light flash lamp (1 mW nominal output power, 10 ms flash separation) of the microplate

183   reader. The experimental stimulation times scale linearly with the flash number (e.g., 2 s for

184   200 flashes (fl)). Wavelength was adjusted using optical filters (BMG Labtech; 445 ± 7.5 nm,

185   480 ± 7.5 nm and 540 ± 7.5 nm; center wavelength (λ) ± full width at half-maximum (FWHM)).

186   Each filter was characterized using a white light source and a spectrophotometer (LI-180,

187   Licor). Xenon lamp light output through the filters was measured using a power meter (LP-1,

188   Sanwa). For the illuminated area of 3 mm^2, the continuous illumination power density (I) was

189   1.75, 1.97 and 1.35 mW/cm^2 for 445, 480 and 540 nm continuously over the stimulation time

190   course.

191

Real-time Ca^{2+} measurement

193   The real-time Ca^{2+} mobilization assay employed mtAequorin in pcDNA3.1. HEK293 cells were

194   seeded at a density of 5 x 10^4 cells/well in white 96-well plates and transfected with receptor

195   and reporter at a ratio of 1:1. The next day, culture medium was replaced with Hank's buffered

196   salt solution (HBSS, Sigma) supplemented with 10 µM coelenterazine h (Nanolight) and 10

197   µM 9-*cis*-retinal in experiments with light-activated receptors. Cells were then incubated for 2

198   h at 37°C. Luminescence was measured in the microplate reader. Baseline luminescence

199   values were recorded for 10 cycles (1 s/cycle) before stimulation. Cells were stimulated with

200   light (see above) or ligand at concentrations as described in the main text and figure captions.

201   For YM254890 experiments, cells were incubated with 10 µM YM254890 (AdipoGen Life

202   Sciences) for 2 h at 37°C before measurements.

203

Real-time β-arrestin2 recruitment

Receptor mediated β-arrestin2 recruitment was assessed using a real-time BRET assay detecting energy transfer between Rluc8-tagged receptors and a mVenus-tagged β-arrestin2. HEK293 cells were seeded at a density of 5 x 10^4 cells/well in white 96-well plates and transfected with receptor-Rluc8 and β-arrestin2-mVenus at a ratio of 1:4. Culture medium was changed 6 h after transfection and supplemented with 10 μM 9-*cis*-retinal (Sigma) for experiments with light-activated receptors. The next day, culture medium was replaced with 40 μl HBSS supplemented and 10 μM 9-*cis*-retinal for experiments with light-activated receptors. Cells were incubated for 1 h at 37°C. Coelenterazine h was added at a final concentration of 5 μM immediately before measurements. Baseline values were recorded for 8 cycles (90 s/cycle) before stimulation. Cells were stimulated with light (see above) or ligand at concentrations as described in the main text and figure captions. BRET measurements were obtained in the microplate reader using 460 (Rluc8) and 520 nm (mVenus) filters. The BRET ratio was calculated by dividing the emission at 520 nm by the emission at 460 nm.

218

Immunofluorescence (IF)

HEK293 cells were seeded on glass coverslips coated with poly-L-ornithine (Sigma) in clear 12-well plates (3 x 10^5 cells/well) and transfected with 1000 ng receptor plasmid. The next day, under dim red light, cells were washed once with pre-warmed PBS and then fixed with 4% PFA for 10 min at RT. Cells were washed again three times with PBS and blocked with PBS + 0.1% Tween (PBS-T) containing 3% BSA at 37°C for 1 h. Cells were incubated with primary antibody (mouse anti-4D2, 1:500 dilution; Abcam, ab98887) at 4°C o/n, washed three times with PBS, and incubated with secondary antibody (donkey anti-mouse, Alexa488 conjugated, 1:750 dilution; Thermo Fisher Scientific, A21202) at RT for 2 h. Cells were then washed once with PBS, incubated with DAPI (Life Technologies) at a final dilution of 1:4000 at RT for 5 min and washed twice with PBS. Coverslips were mounted on microscopy slides using Mowiol mounting medium (Sigma) and left to dry. Images were acquired using a inverted confocal microscope (C1, Nikon) paired with a Plan Apo VC 60x objective. Cells were imaged at 405 and 488 nm with a scan speed of 21.6 frames per s (caution was taken to avoid oversaturation at both 405 (HV = 74, laser power = 4.2) and 488 nm (HV = 82, laser power = 4.2).

235

Flow cytometry (FC)

HEK293 cells were seeded in clear 6-well plates at a density of 1 x 10^6 cells/well and transfected with 2000 ng receptor plasmid. The next day, under dim red light, cells were washed once with PBS and dispersed using Accutase (Sigma) at 37°C for 15 min. Accutase

240 was neutralized using complete medium before the cell suspension was collected in a 15 ml

241 tube and centrifuged. After removal of supernatant, cells were fixed in 2% PFA at 37°C for 10

242 min and washed once with PBS. We choose permeabilizing fixation conditions for

243 quantification of total expression levels. Cells were permeabilized with ice-cold methanol on

244 ice for 30 min. Cells were washed twice in FC buffer (PBS supplemented with 2% FBS) and

245 incubated with primary antibody (see above) at RT for 30 min. Cells were then washed once

246 with FC buffer and incubated with secondary antibody (see above) at RT for 30 min. Samples,

247 including mock transfected, unstained and secondary antibody controls, were run on the same

248 day on a LSR Fortessa X-20 Cytometer (BD Biosciences) and data was analyzed using

249 FlowJo software (Flowjo).

250

251 **Comparison of sequence and structure alignments**

252 Initial comparisons of sequence alignments and structure alignments were performed on rho

253 (PDB ID: 6CMO) and β_2AR (PDB ID: 3SN6) using only the receptor chain (chain R).

254 FATCAT2.0 alignments were performed using the pairwise alignment option of the

255 FATCAT2.0 server[50] (https://fatcat.godziklab.org). Cα atoms were included in the alignments

256 with default alignment parameters. Alignments were manually inspected to determine whether

257 key motifs (E/DRY, CWxP or NPxxY) were correctly paired between the first and the second

258 receptor (e.g., Asp^{3x49} of E/DRY of rho should be paired with Asp^{3x49} of E/DRY of β_2AR).

259   Sequence alignments were performed in MUSCLE as previously[47,51,52] using the

260 sequence of residues that are resolved in the PDB file to enable comparison to structure

261 alignments.

262   For detailed comparison of FATCAT2.0 and MUSCLE alignments, rho (PDB ID:

263 6CMO) was also aligned to A_{2A}R (PDB ID: 6GDF), β1AR (PDB ID: 7JJO) and M_1R (PDB ID:

264 6OIJ) followed by quantification of identical pairs in macros written in Igor Pro (Wavemetrics)

265 (**Supplementary Fig. S1**). These MUSCLE and FATCAT2.0 alignments were in a final step

266 manually analyzed to assess whether OptoXR boundaries were at identical positions

267 **Supplementary Fig. S2**).

268

269 **GPCR-G-protein interacting residues and visualization**

270 GPCR residues in proximity to the Gα subunit were determined in PyMol as described in the

271 main text and figure captions. If available, multiple receptor structures were analyzed to

272 include all possible binding residues as listed in the figure captions. The obtained molecular

273 contact maps were verified using a second and fully automated software (CMView[53]). PDB

274 IDs of the analyzed structures were as follows for the studied receptors: Rho (6CMO, 6OYA),

275 β_2AR (3SN6, 7BZ2) and A_{2A}R (6GDF). Molecular structure images were generated in PyMol.

276

277 **Data analysis and statistics**

278 All pharmacological data were analysed using Prism (9.0, GraphPad). Dose-response data

279 were generated by applying a three-parameter non-linear equation to data extracted from time

280 courses. EC50 values were determined by fitting dose-response data with a sigmoid curve.

281 Statistical measures are provided in the figure captions.

282

283

284 **RESULTS**

285 **Comparison of sequence- and structure-based alignments**

286 The creation of protein chimeras, such as OptoXRs, hinges on the exchange of functionally-

287 equivalent domains between proteins. This is generally achieved by first aligning the proteins

288 of interest, either as primary sequences or as three-dimensional structures, followed by

289 identification of domain boundaries. Engineering of previous OptoXRs exclusively relied on

290 sequence-based alignments, including the prominent chimeras of rho and adrenergic,

291 dopamine, adenosine or muscarinic acetylcholine receptors (**Supplementary Table**

292 **S1**)[18,47,54]. In a complementary approach, we tested whether alignments of structures would

293 yield chimeric receptors that are different from those generated using sequences. This may

294 indeed be the case due to the additional topological information gained and because sequence

295 similarity between GPCRs from different families can be low (e.g., rho and β_2AR, $A_{2A}R$, β_1AR

296 and M_1R exhibit 20, 21, 22 and 23% sequence identity overall, or 21, 22, 23 and 21% when

297 excluding extra- or intracellular termini, respectively). We performed a quantitative comparison

298 of sequence-based alignments (using MUSCLE as in previous studies[18,47]) and structure-

299 based alignments (using FATCAT2.0[50]). For this analysis, we utilized our own computer code

300 that reports the number of identical residue pairs in two alignments (**Supplementary Fig. S1**).

301 For pairs of rho and β_2AR, $A_{2A}R$, β_1AR and M_1R, we found that sequence- and structure-based

302 alignments differed in ~20 to 40% of residue pairs across the sequence (**Fig. 1c**). To determine

303 if these differences impact the design of OptoXRs, we asked whether alignments were

304 identical at the domain boundaries that were previously utilized to generate these chimeras

305 (**Supplementary Fig. S2a**)[19]. We observed only minimal differences that were limited to one

306 receptor pair (rho:β_1AR) and single residues (**Fig. 1c**, **Supplementary Fig. S2b**). This result

307 confirms that for these prototypical receptors and these domain boundaries the generation of

308 OptoXR scaffolds is insensitive to the alignment method. This may not necessarily apply to all

309 GPCR pairs as, e.g., long ICLs can potentially confound sequence alignments.

310

311 **Receptors designs based on structural GPCR-Gα contacts**

312 After comparison of alignment methods, we went on to redesign a prototypical OptoXR using

313 a structure-guided rationale. We chose β_2AR as the target receptor as it is well characterized

9

314   and has been incorporated in a OptoXR previously (the new OptoXR generated here is
315   compared to the existing Opto-β$_2$AR in detail below). We closely examined structures of β$_2$AR
316   and also of rho in complex with their cognate G-proteins (Gα$_s$ for β$_2$AR and Gα$_{i/t}$ for rho)[36,55,56].
317   Using a distance cutoff of 4 Å, chosen analogously to the first study mapping a GPCR-Gα
318   complex[36], we determined the receptor residues that are in proximity to Gα (see **Fig. 2a-d** for
319   protein structures, and **Supplementary Fig. S3** and **Supplementary Table S2** for listed
320   contacts). We found that these contacts extend away from the cytosolic ICLs upwards on α-
321   helices TM3, TM5 and TM6 by as much as four α-helical turns (**Fig. 2b,d**). This observation
322   prompted us to test if ILCs are sufficient for GPCR coupling. We engineered a rho receptor
323   containing exclusively the ILCs of β$_2$AR (termed Opto-β$_2$AR-Loops) and demonstrated
324   expression and membrane localization in HEK293 cells using flow cytometry (FC) and
325   immunofluorescence (IF) (**Fig. 2e,f**) (sequences of all engineered receptors can be found in
326   **Supplementary Tables S3 and S4**). However, upon light stimulation (λ=480 ± 7.5 nm, I=1.97
327   mW/cm^2, 40 s, 4000 flashes (fl)) no increase in intracellular cAMP levels was observed,
328   indicating that incorporation of these secondary structure elements in this particular chimeric
329   receptor was not sufficient to confer a downstream signaling ability (**Fig. 2g,h**). We then
330   hypothesized that including an as complete as possible ensemble of structural β$_2$AR-Gα$_s$
331   contacts will result in efficient G-protein activation. We therefore designed a variant termed
332   Opto-β$_2$AR-All-In where domain boundaries are placed to include all structural contacts
333   (**Supplementary Fig. S3**, **Supplementary Table S2**). This receptor should not only perform
334   efficiently but also provide a basis for examining the contribution of specific contact residues
335   to function (as will be shown below). We first verified expression and localization of Opto-
336   β$_2$AR-All-In using FC and IF (**Fig. 2e,f**). We then tested receptor function upon light stimulation
337   (λ=480 ± 7.5 nm, I=1.97 mW/cm^2, 40 s, 4000 fl) and found that Opto-β$_2$AR-All-In elicited a
338   pronounced increase of intracellular cAMP levels (>50-fold above baseline) (**Fig. 2g,h**). This
339   result is comparable to ligand-induced β$_2$AR responses in this cell type (see below) and
340   demonstrates that inclusion of structural contacts yielded a chimeric receptor that potently
341   activates downstream signaling. We went on to further characterize the rationally-designed
342   Opto-β$_2$AR-All-In, which we termed Opto-β$_2$AR-2.0, first in comparison to β$_2$AR, then to a
343   previous OptoXR and finally to variants that exhibit altered contacts.
344
345   **Signaling profile of Opto-β$_2$AR-2.0**
346   We next characterized the signaling profile of Opto-β$_2$AR-2.0 in comparison to β$_2$AR for
347   multiple signaling pathways (**Fig. 3a**). We first investigated intracellular cAMP production in
348   more detail. HEK293 cells expressing Opto-β$_2$AR-2.0 or β$_2$AR were stimulated with light
349   (λ=480 ± 7.5 nm, I=1.97 mW/cm^2, 0.01-10 s, 1-4000 fl) or the potent β-adrenoreceptor agonist
350   isoproterenol (ISO) followed by real-time cAMP detection (**Fig. 3b**). Generally, cAMP levels

351 reached upon Opto-β_2AR-2.0 activation were similar to those reached upon β_2AR activation,

352 and both receptors exhibited dose-dependent increases (half-maximal activation light dose

353 (LD50) for Opto-β_2AR-2.0: 17 fl (0.17 s, λ=480 ± 7.5 nm, I=1.97 mW/cm^2, EC50 for β_2AR: 8.7

354 nM ISO) (**Fig. 3c,d**). Stimulation of Opto-β_2AR-2.0 and β_2AR induced similar cAMP time

355 courses (**Fig. 3b, Supplementary Fig. S4**).

356 We also investigated the ability of Opto-β_2AR-2.0 and β_2AR to mobilize intracellular

357 Ca^{2+} in response to light or ISO. Analogous to cAMP production, both receptors induced dose-

358 dependent Ca^{2+} signals to similar maximal levels (**Fig. 3e-h**). As for cAMP production, reversal

359 to basal Ca^{2+} levels was marginally more rapid for Opto-β_2AR-2.0 than β_2AR (**Fig. 3e,g**).

360 GPCRs can induce intracellular Ca^{2+} mobilization through multiple pathways, including the

361 canonical Gα_q axis. To test whether β_2AR and Opto-β_2AR-2.0 activate Ca^{2+} *via* this axis, we

362 applied the Gα_q inhibitor YM254890 (YM)[57] and found that it indeed abolished signaling

363 downstream of both receptors (**Fig. 3e,g**).

364 The general agreement between Opto-β_2AR-2.0 and β_2AR signaling observed for G-

365 protein dependent pathways did strikingly not extend to β-arrestin. β_2AR, like many other

366 GPCRs, exhibits the ability to induce outcomes downstream of G-proteins and β-arrestin in a

367 ligand-dependent manner. We quantified β-arrestin2 recruitment to β_2AR and Opto-β_2AR-2.0

368 using sensitive bioluminescence resonance energy transfer assays (BRET) (**Supplementary**

369 **Fig. S5a**). β_2AR recruited β-arrestin2 in a dose-dependent manner with a half-maximal

370 effective ISO dose similar to that observed for cAMP induction (EC50: 18 nM; **Supplementary**

371 **Fig. S5b,c**). However, we did not observe any light-dependent β-arrestin recruitment for Opto-

372 β_2AR-2.0 even at high light doses (λ=480 ± 7.5 nm, I=1.97 mW/cm^2, 40 s, 4000 fl)

373 (**Supplementary Fig. S5d**) pointing to a preference of Opto-β_2AR-2.0 for Gα-coupled

374 pathways. It is noteworthy that β-arrestin recruitment has not been examined in earlier studies

375 of β_2AR OptoXRs (as discussed below). The result that β_2AR and a β_2AR OptoXR receptor

376 exhibit distinct behavior may not be entirely surprising. TM domains contribute to active state

377 conformations and kinetics and ultimately signaling bias[58-60] and these domains are different

378 in β_2AR and the rho chimera. Collectively, we found striking similarities but also differences in

379 in the signaling responses elicited by Opto-β_2AR-2.0 and β_2AR.

380

381 **Optical activation profile and comparison to earlier Opto-β_2AR**

382 We went on to characterize the optical activation profile of Opto-β2AR and also compared it

383 to an earlier β_2AR OptoXR[18,19,26]. We found that whilst light stimulation for 2 s (λ=480 ± 7.5

384 nm, I=1.97 mW/cm^2, 200 fl) was required to produce saturating cAMP levels, even a single 10

385 ms light flash induced a signal that was sizeable (~10% of maximal cAMP induction) and

386 transient (decay in 7.5 min and thus faster than the decay after application of the amplitude-

387 equivalent dose of 10 nM ISO) (**Fig. 4a**, **Supplementary Fig. S4**). Opto-β_2AR-2.0 employs

388 rho as light-sensing photoreceptor core which is sensitive to blue-green light across a relatively

389 broad wavelength range (maximal absorption wavelength: 500 nm, FWHM: ~100 nm)[61,62]. We

390 confirmed the spectral sensitivity of Opto-β_2AR-2.0 by stimulating cells with light of different

391 wavelengths (**Fig. 4b**). As expected given the broad absorption peak, Opto-β_2AR-2.0 could be

392 activated at 480 ± 7.5 nm (the closest wavelength to 500 nm available to us; I=1.97 mW/cm^2)

393 as well as at 445 ± 7.5 nm and 540 ± 7.5 nm (I=1.75 and 1.35 mW/cm^2, 0.01-10 s, 1-1000 fl).

394   In the seminal study of Kim *et al.*[19], a β_2AR OptoXR was designed using a screening

395 approach and this receptor was later expressed *in vivo* and *ex vivo*[18,26]. Following the current

396 convention, we refer to this earlier receptor as Opto-β_2AR whilst our receptors carry further

397 labels (e.g., the label 2.0; the domain boundaries of Opto-β_2AR and Opto-β_2AR-2.0 shown

398 side-by-side in **Supplementary Fig. S3**). We compared the efficiency of Opto-β_2AR-2.0 to

399 Opto-β_2AR and found that Opto-β_2AR-2.0 generated larger maximal signals (by 7.2 fold) and

400 produced half-maximal signals at 4.8-fold lower light doses (**Fig. 4c**) (LD50 of Opto-β_2AR: 82

401 fl, 0.82s; LD50 of Opto-β_2AR-2.0: 17 fl, 0.17s; in both cases λ=480 ± 7.5 nm, I=1.97 mW/cm^2;

402 expression levels were comparable, **Supplementary Fig. S6**). On the time scale of our

403 longest repetition experiments (~1.5 h), cAMP signals generated by Opto-β_2AR-2.0 were even

404 comparable to the potent jellyfish opsin JellyOp[16] (**Supplementary Fig. S7**). One further

405 notable observation was that the activity of Opto-β_2AR, but not that of Opto-β_2AR-2.0 or β_2AR,

406 was sensitive to the Gα_i inhibitor PTX (**Supplementary Fig. S8**). This result suggests that the

407 original Opto-β_2AR exhibited a signaling activity that is in this cell type not representative of

408 β_2AR but may be relevant in the context of previous and future applications of this earlier

409 receptor. Understanding the mechanism underlying this activity requires separate further

410 study as it cannot be attributed to the absence/presence of structural GPCR-Gα contacts: (i)

411 no rho-G$\alpha_{i/o/t}$ contact residues remain in Opto-β_2AR (**Supplementary Fig. S3**) and (ii) Gα_s and

412 Gα_i associate with the homologous β_1AR receptor through an overlapping ensemble of

413 residues[63] all of which are present in β_2AR and Opto-β_2AR-2.0. While the effect of PTX was

414 pronounced, cAMP production by Opto-β_2AR even under conditions of Gα_i inhibition was still

415 several fold below that of Opto-β_2AR-2.0 (**Supplementary Fig. S8**). Collectively, these data

416 show that Opto-β_2AR-2.0 is an efficient optical actuator that offers higher potency and

417 specificity than its closest known OptoXR relative.

418

419 **Contributions of contact residues to Opto-β_2AR-2.0 function**

420 We next tested if the functional contribution of individual structural contacts can be quantified

421 in Opto-β_2AR-2.0. We examined key residues that (i) are located in the three main receptors

422 domains that were exchanged between rho and β_2AR (TM3-ICL2-TM4, TM5-ICL3-TM6 and

423 TM7-C), (ii) form contacts (e.g., hydrophobic interactions or charge-charge interactions) to Gα_s

424 and (iii) are present in Opto-β_2AR-2.0 but absent in Opto-β_2AR. In the domains TM3-ICL2-

425   TM4 and TM5-ICL3-TM6, we focused on I139^{3x54} and L270^{6x37} that form hydrophobic contacts

426   to Gα$_s$ (in both cases through Cδ side chain atoms[36]; residue numbers correspond to the Opto-

427   β$_2$AR-2.0 sequence and, in superscript, to the GPCRdb numbering scheme[64]). Upon

428   substitution of these residues to the corresponding rho residues present in Opto-β$_2$AR

429   (I139^{3x54}V and L270^{6x37}V; Val does not contain a Cδ atom), we found reduced cAMP induction

430   by 15 and 25% as well as ~2-fold reduced LD50 values (33.3 fl, 0.34 s and 32.9 fl, 0.33 s,

431   respectively; in both cases λ=480 ± 7.5 nm, I=1.97 mW/cm^2) (**Fig. 4d**). A I139^{3x54}V L270^{6x37}V

432   double mutant resulted in further loss of function (LD50 34.4 flashes, 0.35 s, 44% reduced

433   cAMP induction) (**Fig. 4d**). We also investigated TM7. Specifically, residue R335^{7x55} at the

434   cytoplasmic end of this TM α-helix has been implicated in Gα$_s$-binding through a charge-

435   charge contact to residue E392$^{H5.24}$ of Gα$_s$ in structural studies and molecular dynamics

436   simulations[43,65]. A deleterious substitution (R335L^{7x55}; modelled after a naturally observed

437   receptor variant[66]) resulted in maximal cAMP levels that were reduced by 42% (LD50: 36.6 fl,

438   0.37s, λ=480 ± 7.5 nm, I=1.97 mW/cm^2) (**Fig. 4e**). Overall, the function of Opto-β$_2$AR-2.0 is

439   indeed sensitive to substitution of newly-introduced residues that were identified in structural

440   GPCR-Gα complex analysis.

441

442   **Structure-guided receptors as a development platform**

443   We went on to demonstrate consequences of the optimization approach. Above exploration

444   of contact residues was assisted by the large signals generated by Opto-β$_2$AR-2.0: A

445   quantitative analysis could still be performed despite a marked reduction in activity because

446   of residue substitutions. We reasoned that the potency of Opto-β$_2$AR-2.0 may also enable

447   experiments where the photosensitive domain of the receptor is engineered as also this

448   manipulation may be associated with reduced function. Of importance in optogenetic tool

449   development is an availability of actuator proteins with sensitivities to different wavelengths

450   ("blue-shifting" (towards lower maximal absorption wavelengths) or "red-shifting" (towards

451   higher maximal absorption wavelengths))[67-70]. This is generally achieved either through

452   identification of naturally-occurring spectrally-diverse photoreceptors, e.g. cone opsins in the

453   case of GPCRs[11], or through tuning of photoreceptors using substitutions in their chromophore

454   binding pockets[71,72]. Binding pocket mutagenesis can be associated with reduced function in

455   opsins[73-76], which is one possible reason why spectral tuning using mutagenesis has never

456   been demonstrated in OptoXRs. Indeed, when introducing three substitutions in the original

457   Opto-β$_2$AR that were previously shown to blue-shift rho absorption by ~50 nm[75] (T118^{3x33}A,

458   E122^{3x37}D and A318^{7x39}S; residue numbers correspond to Opto-β$_2$AR-2.0/GPCRdb

459   numbering; **Fig. 5a**), no light-induced activity could be detected (λ=480 ± 7.5 nm, I=1.97

460   mW/cm^2, 0.01-10 s, 1-1000 fl) (**Fig. 5b**). In turn, introduction of the same residues in Opto-

461   β$_2$AR-2.0 resulted in a blue-shifted variant (termed Opto-β$_2$AR-2.0-Blue) that induced cAMP

462   to levels that were comparable to previous non-shifted OptoXRs (λ=480 ± 7.5 nm, I=1.97

463   mW/cm^2, 0.01-10 s, 1-1000 fl) (**Fig. 5c**). As expected, in the spectrally tuned Opto-β$_2$AR-2.0-

464   Blue sensitivity to blue light was maximal and to green light reduced (**Fig. 5c**).

465   We also explored whether a GPCR-Gα contact-based redesign may be applicable to

466   a further receptor (**Fig. 5d**). We have previously developed a light-activated A$_{2A}$R (Opto-A$_{2A}$R)

467   and characterized its function in highly-sensitive because integrative transcriptional reporter

468   assays[47]. Analogously as for Opto-β$_2$AR-2.0 above, we determined G-protein proximal

469   residues in the A$_{2A}$R receptor structure[38] to inform the placement of domain boundaries

470   following the "All-In"-rationale. We termed the resulting receptor Opto-A$_{2A}$R-2.0. Opto-A$_{2A}$R-

471   2.0 also contained additional A$_{2A}$R residues in TM3, TM6 and the C-terminus when compared

472   to Opto-A$_{2A}$R (**Supplementary Tables S3 and S4**). We went on to test the ability of both

473   receptors to induce cAMP responses and found that only Opto-A$_{2A}$R-2.0 resulted in detectable

474   activation in the real-time assays (**Fig. 5e,f**). Thus the structure-guided approach permitted

475   generation of a functionally improved A$_{2A}$R OptoXR.

476

477

478   **DISCUSSION**

479   GPCRs relay diverse extracellular signals to specific downstream signaling pathways and

480   thereby regulate essential physiology. To control GPCR signaling with spatio-temporal

481   precision, chimeric light-activated OptoXRs have been developed and deployed alongside

482   repurposed naturally-occurring opsins[20,21]. The design of most published OptoXRs relied on

483   domain boundaries that were proposed in a seminal study[19]. Notably, this recipe was

484   formulated at a time when few high-resolution structures were available for GPCRs and none

485   for GPCR-G-protein complexes. The past fifteen years have seen the emergence of detailed

486   structures depicting >150 unique GPCRs and >50 unique GPCR-signaling-protein

487   complexes[1,30]. Here, we utilized some of this structural information for rational improvement of

488   OptoXRs. First, we evaluated if sequence alignments and structure alignments yield the same

489   chimeric receptor backbones. For our set of prototypical receptors and domain boundaries this

490   was the case. Second, we identified receptor residues that are proximal to Gα-subunits to

491   position the domain boundaries in modified chimeric receptors. We found that an "All-In"-

492   rationale, which incorporates the three ILCs, the C-terminus and the identified structural

493   GPCR-Gα contact regions, markedly improved the function of a β$_2$AR OptoXR. These

494   modifications, along with a non-functional chimeric receptor that contained only the ICLs of

495   β$_2$AR, demonstrated how TM α-helical residues contribute to efficient downstream coupling.

496   As we incorporated all residues identified in the complex structure, a rationale for further

497   optimization is not directly evident (see below for a test of the contribution of inserted residues).

498   The approach we have taken is structure-based and thus fundamentally different from, e.g.,

14

499   the screening-based methods employed on OptoXRs previously or on GPCR-based

500   fluorescent sensors. In Opto-β_2AR-2.0, many of the incorporated TM α-helical residues (e.g.,

501   I139^{3x54}, L280^{6x37} or R335^{7x55}) are conserved in Gα_s-coupled aminergic (including adrenergic)

502   receptors but not in non-Gα_s-coupled receptors. Our comparison of Opto-β_2AR-2.0 and a

503   previous Opto-β_2AR, which retained rho residues at the corresponding sites, and a reverse

504   experiment in which we substituted these residues in Opto-β_2AR-2.0, confirmed their

505   contributions to function. In addition, our analysis also rationalizes previous findings that

506   omission of larger structural domains of β_2AR, e.g. entire intracellular domains, resulted in

507   reduced activity of chimeric GPCRs[16,19,27].

508   Our work is complementary to two elegant recent studies in which coupling

509   downstream of GPCRs was altered using structural information. Using simulations of terminal

510   Gα α-helices in combination with functional assays, Sandhu *et al.* generated a triple mutant

511   adrenoreceptor with more promiscuous downstream coupling, in particular leading to more

512   potent activation of Gα_q compared to the WT receptor[43]. Using structure modeling and *in silico*

513   and experimental mutagenesis, Young *et al.* engineered orthogonal receptor-Gα-pairs that

514   interacted specifically and independently of their endogenous counterparts[42]. Collectively,

515   these studies and our work demonstrate separate advances towards several design objectives

516   (coupling switch, promiscuity or orthogonality) using distinct strategies (chimeric receptors or

517   mutagenesis).

518   One element of our study was examination to which degree this OptoXR recapitulates

519   the function of the ligand-activated target receptor. GPCRs assume distinct ligand-dependent

520   active states and state lifetimes that lead to preferred activation of some of the available

521   signaling pathways over others[58-60,77-79]. OptoXR activation likewise was associated with a

522   particular signaling profile. Given pronounced differences between rho and β_2AR, it may not

523   be surprising that the signaling profile of Opto-β_2AR-2.0 was not identical to that of β_2AR. In

524   particular, we were unable to detect β-arrestin recruitment for Opto-β_2AR-2.0 and thus under

525   the conditions examined here the activity of Opto-β_2AR-2.0 resembled that of β_2AR in

526   response to G-protein-biased ligands, such as pepducins[80]. It is noteworthy that an ability to

527   predominantly activate G-protein pathways may be desirable in some physiological

528   scenarios[80,81]. This result may also be relevant in the context of an earlier study that proposed

529   the development of a "functionally-selective" Opto-β_2AR with limited Gα_s signaling but

530   induction of pathways that are known to be downstream of β-arrestin[26]. Notably, β-arrestin

531   recruitment was not explored in this study and selectivity was achieved through mutagenesis

532   of key functional motifs which were (i) located within the rho core and (ii) present in most Class

533   A GPCRs (e.g., the highly-conserved Tyr^{3x51} of the E/DRY motif or a further tyrosine (Tyr^{5x58})

534   that participates in active-state-specific interactions)[26,31]. Because of the placement of these

15

535   substitutions in rho domains (as opposed to in β_2AR-derived domains as here), a comparison

536   of the previous results and ours is not possible.

537   The large signaling response elicited by Opto-β_2AR-2.0 prompted us to explore further

538   capabilities of OptoXRs. We introduced a spectral absorption shift to the rho core of Opto-

539   β_2AR-2.0 to diversify function. The blue-shifted receptor may complement blue-light sensitive

540   cone opsins that activate opposing signaling responses (G$\alpha_{i/o}$ instead of Gα_s)[11]. Mutagenesis

541   in binding pockets are associated with reduced protein folding and function in many protein

542   families including opsins[73-76]. Indeed, we observed that substitution of three residues in

543   proximity of the retinal cofactor impacted the function of the original Opto-β_2AR such that we

544   were not able to detect changes in cAMP levels. In contrast, Opto-β_2AR-2.0-Blue induced

545   changes that were even comparable to those produced by earlier unperturbed OptoXRs.

546   Finally, again prompted by the functional improvement observed in Opto-β_2AR-2.0, we went

547   on to show that a structure-guided approach can also be applied to generate Opto-A$_{2A}$R-2.0.

548   Structural biology has had a profound impact on the field of optogenetics, e.g. by

549   enabling the rational design of light-activated ion channels, enzymes and protein-protein

550   interactions[71,73,82]. We show that rational exchange of receptor domains resulted in more

551   potent OptoXRs and enabled OptoXRs with new functions. However, because this is the first

552   demonstration of structure-guided coupling engineering in OptoXRs, and one of very few in

553   GPCRs in general[42,43], further studies are required to test how universal this approach is. It is

554   interesting to note that the temporal sequence of events driving the association of the G-

555   protein to a GPCR is an active area of study. It is possible that this association initially involves

556   intermediate receptor states and consequently contacts other than those observed in the

557   stable GPCR-G-protein complexes; however, such contacts have not yet been identified[65,83,84]

558   and thus cannot be incorporated in a receptor design. OptoXRs may in the future support time-

559   resolved studies of these binding events by providing non-invasive activation tools, similarly

560   to successful photoreceptor applications in spectroscopy or drug discovery[85,86]. In addition to

561   serving as an experimental platform, targeted OptoXRs may also continue to make

562   contributions towards understanding the impact of signaling on cells and cellular networks.

AUTHOR CONTRIBUTIONS

Conceptualization, A.M.T., E.J.G. and H.J.; Funding Acquisition, E.J.G. and H.J.; Methodology, A.M.T., W.L.S., E.J.G. and H.J.; Project Administration, H.J.; Investigation, A.M.T., W.L.S. and E.J.G.; Data curation, A.M.T., W.L.S., E.J.G. and H.J.; Supervision, E.J.G. and H.J.; Writing - Original Draft, A.M.T. and H.J.; Writing - Review and Editing, H.J.

CONFLICT OF INTEREST

The authors declare no conflict of interest.

REFERENCES

1. Kooistra, A.J. et al. GPCRdb in 2021: integrating GPCR sequence, structure and function. *Nucleic Acids Res* **49**, D335-D343 (2021).

2. Insel, P.A. et al. GPCRomics: An approach to discover GPCR drug targets. *Trends Pharmacol Sci* **40**, 378-387 (2019).

3. Sriram, K. & Insel, P.A. G Protein-Coupled Receptors as Targets for Approved Drugs: How Many Targets and How Many Drugs? *Mol Pharmacol* **93**, 251-258 (2018).

4. Hauser, A.S., Attwood, M.M., Rask-Andersen, M., Schioth, H.B. & Gloriam, D.E. Trends in GPCR drug discovery: new agents, targets and indications. *Nat Rev Drug Discov* **16**, 829-842 (2017).

5. Flock, T. et al. Selectivity determinants of GPCR-G-protein binding. *Nature* **545**, 317-322 (2017).

6. Atwood, B.K., Lopez, J., Wager-Miller, J., Mackie, K. & Straiker, A. Expression of G protein-coupled receptors and related proteins in HEK293, AtT20, BV2, and N18 cell lines as revealed by microarray analysis. *BMC Genomics* **12**, 14 (2011).

7. Oldham, W.M. & Hamm, H.E. Heterotrimeric G protein activation by G-protein-coupled receptors. *Nat Rev Mol Cell Biol* **9**, 60-71 (2008).

8. Marti-Solano, M. et al. Combinatorial expression of GPCR isoforms affects signalling and drug responses. *Nature* **587**, 650-656 (2020).

9. Tichy, A.M., Gerrard, E.J., Sexton, P.M. & Janovjak, H. Light-activated chimeric GPCRs: limitations and opportunities. *Curr Opin Struct Biol* **57**, 196-203 (2019).

10. Kleinlogel, S. Optogenetic user's guide to Opto-GPCRs. *Front Biosci* **21**, 794-805 (2016).

11. Masseck, O.A. et al. Vertebrate cone opsins enable sustained and highly sensitive rapid control of Gi/o signaling in anxiety circuitry. *Neuron* **81**, 1263-73 (2014).

12. Karunarathne, W.K., Giri, L., Kalyanaraman, V. & Gautam, N. Optically triggering spatiotemporally confined GPCR activity in a cell and programming neurite initiation and extension. *Proc Natl Acad Sci U S A* **110**, E1565-74 (2013).

13. Li, X. et al. Fast noninvasive activation and inhibition of neural and network activity by vertebrate rhodopsin and green algae channelrhodopsin. *Proc Natl Acad Sci USA* **102**, 17816-21 (2005).

14. Copits, B.A. et al. A photoswitchable GPCR-based opsin for presynaptic inhibition. *Neuron* **109**, 1791-1809 e11 (2021).

15. Mahn, M. et al. Efficient optogenetic silencing of neurotransmitter release with a mosquito rhodopsin. *Neuron* **109**, 1621-1635 e8 (2021).

16. Bailes, H.J., Zhuang, L.Y. & Lucas, R.J. Reproducible and sustained regulation of Galphas signalling using a metazoan opsin as an optogenetic tool. *PLoS One* **7**, e30774 (2012).

17. Zemelman, B.V., Lee, G.A., Ng, M. & Miesenbock, G. Selective photostimulation of genetically chARGed neurons. *Neuron* **33**, 15-22 (2002).

18. Airan, R.D., Thompson, K.R., Fenno, L.E., Bernstein, H. & Deisseroth, K. Temporally precise in vivo control of intracellular signalling. *Nature* **458**, 1025-9 (2009).

19. Kim, J.M. et al. Light-driven activation of beta 2-adrenergic receptor signaling by a chimeric rhodopsin containing the beta 2-adrenergic receptor cytoplasmic loops. *Biochemistry* **44**, 2284-92 (2005).

20. Wiegert, J.S., Mahn, M., Prigge, M., Printz, Y. & Yizhar, O. Silencing neurons: tools, applications, and experimental constraints. *Neuron* **95**, 504-529 (2017).

21. Spangler, S.M. & Bruchas, M.R. Optogenetic approaches for dissecting neuromodulation and GPCR signaling in neural circuits. *Curr Opin Pharmacol* **32**, 56-70 (2017).

22. Iwai, Y. et al. Transient astrocytic Gq signaling underlies remote memory enhancement. *Front Neural Circuits* **15**, 658343 (2021).

636 23. van Wyk, M., Pielecka-Fortuna, J., Lowel, S. & Kleinlogel, S. Restoring the ON switch
637   in blind retinas: Opto-mGluR6, a next-generation, cell-tailored optogenetic tool. *PLoS*
638   *Biol* **13**, e1002143 (2015).
639 24. Xu, Y. et al. Optogenetic control of chemokine receptor signal and T-cell migration.
640   *Proc Natl Acad Sci U S A* **111**, 6371-6 (2014).
641 25. Siuda, E.R. et al. Spatiotemporal control of opioid signaling and behavior. *Neuron* **86**,
642   923-35 (2015).
643 26. Siuda, E.R. et al. Optodynamic simulation of beta-adrenergic receptor signalling. *Nat*
644   *Commun* **6**, 8480 (2015).
645 27. Hickey, D.G. et al. Chimeric human opsins as optogenetic light sensitisers. *J Exp Biol*
646   **224**(2021).
647 28. Berry, M.H. et al. Restoration of high-sensitivity and adapting vision with a cone opsin.
648   *Nat Commun* **10**, 1221 (2019).
649 29. Cehajic-Kapetanovic, J. et al. Restoration of vision with ectopic expression of human
650   rod opsin. *Curr Biol* **25**, 2111-22 (2015).
651 30. Congreve, M., de Graaf, C., Swain, N.A. & Tate, C.G. Impact of GPCR structures on
652   drug discovery. *Cell* **181**, 81-91 (2020).
653 31. Zhou, Q. et al. Common activation mechanism of class A GPCRs. *Elife* **8**(2019).
654 32. Wootten, D., Christopoulos, A., Marti-Solano, M., Babu, M.M. & Sexton, P.M.
655   Mechanisms of signalling and biased agonism in G protein-coupled receptors. *Nat Rev*
656   *Mol Cell Biol* **19**, 638-653 (2018).
657 33. Weis, W.I. & Kobilka, B.K. The Molecular Basis of G Protein-Coupled Receptor
658   Activation. *Annu Rev Biochem* **87**, 897-919 (2018).
659 34. Gurevich, V.V. & Gurevich, E.V. Molecular mechanisms of GPCR signaling: A
660   structural perspective. *Int J Mol Sci* **18**(2017).
661 35. Venkatakrishnan, A.J. et al. Diverse activation pathways in class A GPCRs converge
662   near the G-protein-coupling region. *Nature* **536**, 484-7 (2016).
663 36. Rasmussen, S.G. et al. Crystal structure of the beta2 adrenergic receptor-Gs protein
664   complex. *Nature* **477**, 549-55 (2011).
665 37. Munk, C. et al. An online resource for GPCR structure determination and analysis. *Nat*
666   *Methods* **16**, 151-162 (2019).
667 38. Garcia-Nafria, J., Lee, Y., Bai, X., Carpenter, B. & Tate, C.G. Cryo-EM structure of the
668   adenosine A2A receptor coupled to an engineered heterotrimeric G protein. *Elife*
669   **7**(2018).
670 39. Liang, Y.L. et al. Phase-plate cryo-EM structure of a class B GPCR-G-protein complex.
671   *Nature* **546**, 118-123 (2017).
672 40. Glukhova, A. et al. Rules of engagement: GPCRs and G proteins. *ACS Pharm Transl*
673   *Sci* **1**, 73-83 (2018).
674 41. Keri, D. & Barth, P. Reprogramming G protein coupled receptor structure and function.
675   *Curr Opin Struct Biol* **51**, 187-194 (2018).
676 42. Young, M. et al. Computational design of orthogonal membrane receptor-effector
677   switches for rewiring signaling pathways. *Proc Natl Acad Sci U S A* **115**, 7051-7056
678   (2018).
679 43. Sandhu, M. et al. Conformational plasticity of the intracellular cavity of GPCR-G-protein
680   complexes leads to G-protein promiscuity and selectivity. *Proc Natl Acad Sci U S A*
681   **116**, 11956-11965 (2019).
682 44. Nakajima, K. & Wess, J. Design and functional characterization of a novel, arrestin-
683   biased designer G protein-coupled receptor. *Mol Pharmacol* **82**, 575-82 (2012).
684 45. Guettier, J.M. et al. A chemical-genetic approach to study G protein regulation of beta
685   cell function in vivo. *PNAS* **106**, 19197-202 (2009).
686 46. Savage, E.E., Wootten, D., Christopoulos, A., Sexton, P.M. & Furness, S.G. A simple
687   method to generate stable cell lines for the analysis of transient protein-protein
688   interactions. *Biotechniques* **54**, 217-21 (2013).
689 47. Morri, M. et al. Optical functionalization of human class A orphan G-protein-coupled
690   receptors. *Nat Commun* **9**, 1950 (2018).

48. Tang, Y. et al. Identification of the endophilins (SH3p4/p8/p13) as novel binding partners for the beta1-adrenergic receptor. *Proc Natl Acad Sci U S A* **96**, 12559-64 (1999).

49. Tichy, A.M., Gerrard, E.J., Legrand, J.M.D., Hobbs, R.M. & Janovjak, H. Engineering strategy and vector library for the rapid generation of modular light-controlled protein-protein interactions. *J Mol Biol* **431**, 3046-3055 (2019).

50. Li, Z., Jaroszewski, L., Iyer, M., Sedova, M. & Godzik, A. FATCAT 2.0: towards a better understanding of the structural diversity of proteins. *Nucleic Acids Res* **48**, W60-W64 (2020).

51. Madeira, F. et al. The EMBL-EBI search and sequence analysis tools APIs in 2019. *Nucleic Acids Res* **47**, W636-W641 (2019).

52. Edgar, R.C. MUSCLE: a multiple sequence alignment method with reduced time and space complexity. *BMC Bioinform* **5**, 113 (2004).

53. Vehlow, C. et al. CMView: interactive contact map visualization and analysis. *Bioinformatics* **27**, 1573-4 (2011).

54. Gunaydin, L.A. et al. Natural neural projection dynamics underlying social behavior. *Cell* **157**, 1535-51 (2014).

55. Gao, Y. et al. Structures of the rhodopsin-transducin complex: Insights into G-protein activation. *Mol Cell* **75**, 781-790 e3 (2019).

56. Kang, Y. et al. Cryo-EM structure of human rhodopsin bound to an inhibitory G protein. *Nature* **558**, 553-558 (2018).

57. Takasaki, J. et al. A novel Galphaq/11-selective inhibitor. *J Biol Chem* **279**, 47438-45 (2004).

58. Lamichhane, R. et al. Biased signaling of the G-Protein-coupled receptor beta2AR is governed by conformational exchange kinetics. *Structure* **28**, 371-377 e3 (2020).

59. McCorvy, J.D. et al. Structure-inspired design of beta-arrestin-biased ligands for aminergic GPCRs. *Nat Chem Biol* **14**, 126-134 (2018).

60. Liu, J.J., Horst, R., Katritch, V., Stevens, R.C. & Wuthrich, K. Biased signaling pathways in beta2-adrenergic receptor characterized by 19F-NMR. *Science* **335**, 1106-10 (2012).

61. Govardovskii, V.I., Fyhrquist, N., Reuter, T., Kuzmin, D.G. & Donner, K. In search of the visual pigment template. *Vis Neurosci* **17**, 509-28 (2000).

62. Partridge, J.C. & De Grip, W.J. A new template for rhodopsin (vitamin A1 based) visual pigments. *Vision Res* **31**, 619-30 (1991).

63. Alegre, K.O. et al. Structural basis and mechanism of activation of two different families of G proteins by the same GPCR. *Nat Stru Mol Biol* **28**, 936-944 (2021).

64. Isberg, V. et al. Generic GPCR residue numbers - aligning topology maps while minding the gaps. *Trends Pharmacol Sci* **36**, 22-31 (2015).

65. Ma, X. et al. Analysis of beta2AR-Gs and beta2AR-Gi complex formation by NMR spectroscopy. *Proc Natl Acad Sci U S A* **117**, 23096-23105 (2020).

66. Hauser, A.S. et al. Pharmacogenomics of GPCR Drug Targets. *Cell* **172**, 41-54 e19 (2018).

67. Forli, A., Pisoni, M., Printz, Y., Yizhar, O. & Fellin, T. Optogenetic strategies for high-efficiency all-optical interrogation using blue-light-sensitive opsins. *Elife* **10**(2021).

68. Hochbaum, D.R. et al. All-optical electrophysiology in mammalian neurons using engineered microbial rhodopsins. *Nat Methods* **11**, 825-33 (2014).

69. Lin, J.Y., Knutsen, P.M., Muller, A., Kleinfeld, D. & Tsien, R.Y. ReaChR: a red-shifted variant of channelrhodopsin enables deep transcranial optogenetic excitation. *Nat Neurosci* **16**, 1499-508 (2013).

70. Tabor, J.J., Levskaya, A. & Voigt, C.A. Multichromatic control of gene expression in Escherichia coli. *J Mol Biol* **405**, 315-24 (2011).

71. Ziegler, T. & Moglich, A. Photoreceptor engineering. *Front Mol Biosci* **2**, 30 (2015).

72. O'Neill, P.R. & Gautam, N. Optimizing optogenetic constructs for control over signaling and cell behaviours. *Photochem Photobiol Sci* **14**, 1578-85 (2015).

73. Deisseroth, K. & Hegemann, P. The form and function of channelrhodopsin. *Science* **357**, 6356 (2017).

74. Singhal, A. et al. Structural role of the T94I rhodopsin mutation in congenital stationary night blindness. *EMBO Rep* **17**, 1431-1440 (2016).

75. Janz, J.M. & Farrens, D.L. Engineering a functional blue-wavelength-shifted rhodopsin mutant. *Biochemistry* **40**, 7219-27 (2001).

76. Lin, S.W. et al. Mechanisms of spectral tuning in blue cone visual pigments. Visible and raman spectroscopy of blue-shifted rhodopsin mutants. *J Biol Chem* **273**, 24583-91 (1998).

77. Wingler, L.M. & Lefkowitz, R.J. Conformational basis of G protein-coupled receptor signaling versatility. *Trends Cell Biol* **30**, 736-747 (2020).

78. Violin, J.D., Crombie, A.L., Soergel, D.G. & Lark, M.W. Biased ligands at G-protein-coupled receptors: promise and progress. *Trends Pharmacol Sci* **35**, 308-16 (2014).

79. Shonberg, J. et al. Biased agonism at G protein-coupled receptors: the promise and the challenges--a medicinal chemistry perspective. *Med Res Rev* **34**, 1286-330 (2014).

80. Carr, R., 3rd et al. Development and characterization of pepducins as Gs-biased allosteric agonists. *J Biol Chem* **289**, 35668-84 (2014).

81. Billington, C.K., Ojo, O.O., Penn, R.B. & Ito, S. cAMP regulation of airway smooth muscle function. *Pulm Pharmacol Ther* **26**, 112-20 (2013).

82. Dagliyan, O. & Hahn, K.M. Controlling protein conformation with light. *Curr Opin Struct Biol* **57**, 17-22 (2019).

83. Ahn, D., Ham, D. & Chung, K.Y. The conformational transition during G protein-coupled receptor (GPCR) and G protein interaction. *Curr Opin Struct Biol* **69**, 117-123 (2021).

84. Du, Y. et al. Assembly of a GPCR-G protein complex. *Cell* **177**, 1232-1242 e11 (2019).

85. Agus, V. & Janovjak, H. Optogenetic methods in drug screening: technologies and applications. *Curr Opin Biotechnol* **48**, 8-14 (2017).

86. Kottke, T., Lorenz-Fonfria, V.A. & Heberle, J. The grateful infrared: Sequential protein structural changes resolved by infrared difference spectroscopy. *J Phys Chem B* **121**, 335-350 (2017).

FIGURES AND FIGURE CAPTIONS

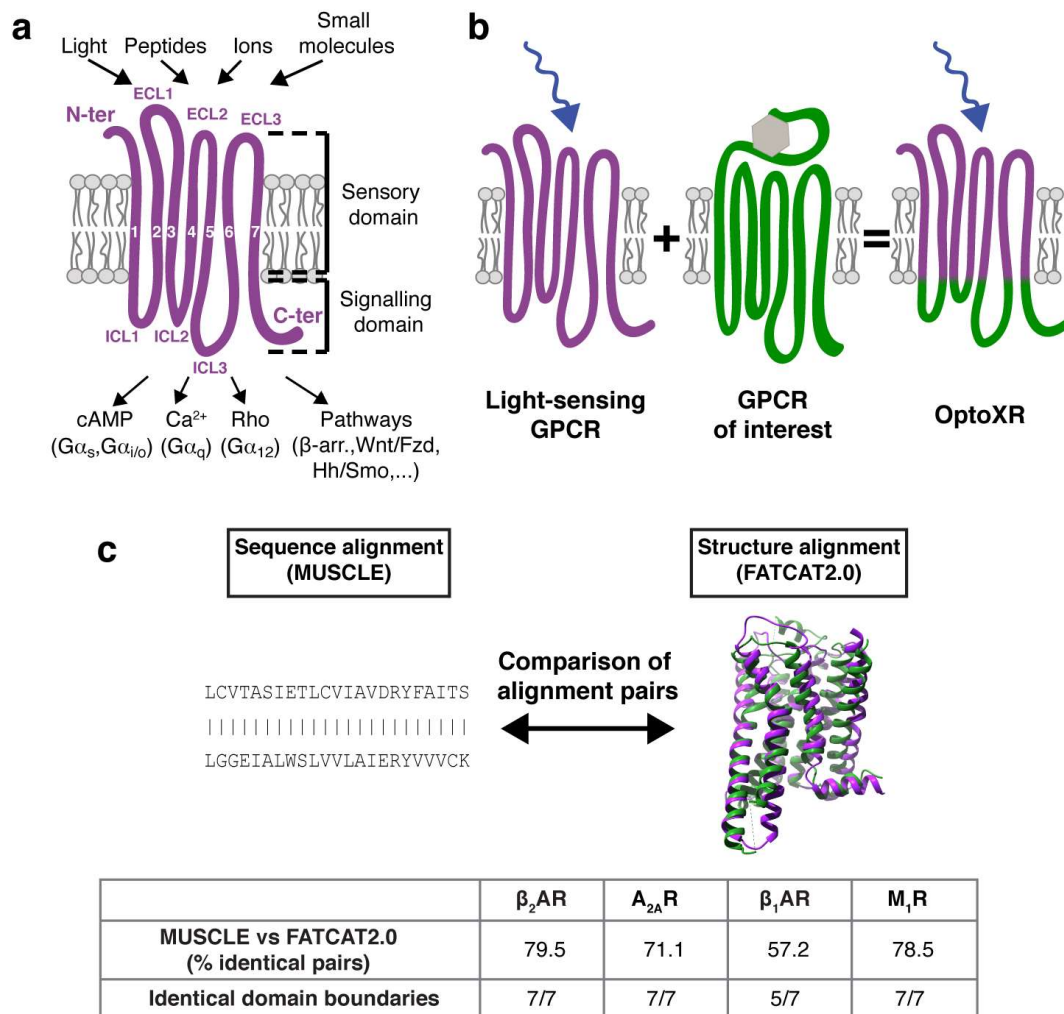|	β_2AR	$A_{2A}R$	β_1AR	M_1R
MUSCLE vs FATCAT2.0 (% identical pairs)	79.5	71.1	57.2	78.5
Identical domain boundaries	7/7	7/7	5/7	7/7

Fig. 1: Functional principle of OptoXRs and alignment methodologies. (a) GPCRs sense a variety of external stimuli using their extracellular and TM domains. Downstream signaling is mediated by residues that face the intracellular environment. **(b)** In chimeric OptoXRs, the signaling elements of a target GPCR of interest is fused to the sensory elements of a light-activated GPCR. **(c)** Top: Sequence- and structure-based alignments were compared. Bottom: Quantification of alignment similarity expressed either as the percentage of identical residue pairs (top row; see **Supplementary Fig. S1** for a definition of residue pairs) or as the number of identical domain boundaries (bottom row; see **Supplementary Fig. S2** for a definition of domain boundaries).
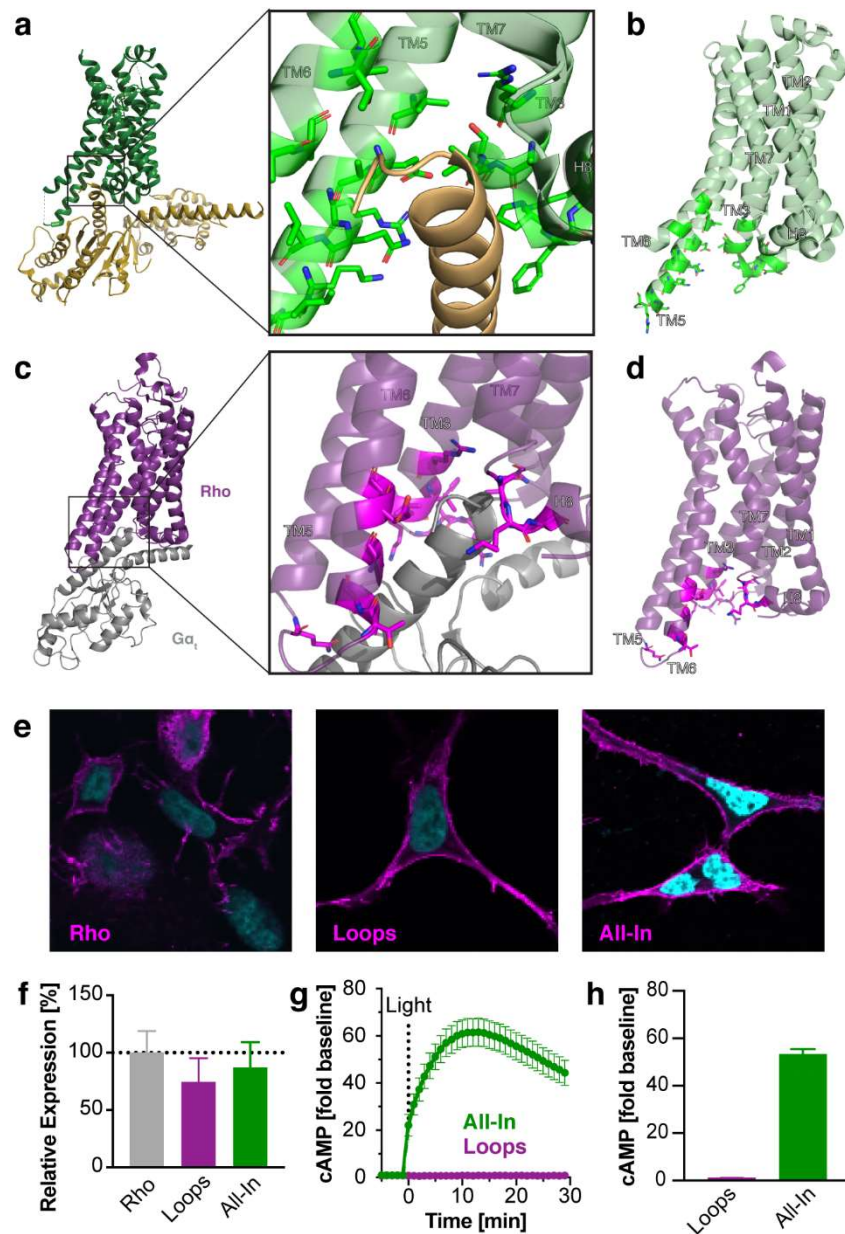
Fig. 2: Identification of functionally-relevant domain boundaries. (a-d) Gα contacts on β$_2$AR (a, b) and rho (c, d) defined as described in the main text (PDB ID: 3SN6 and 6OYA). Contacts extend upwards on TM α-helices. **(e)** Confocal microscopy of rho, Opto-β$_2$AR-Loops and -All-In (N-terminal rho epitope 4D2). **(f)** FC analysis of rho, Opto-β$_2$AR-Loops and -All-In expression using the same antibody as in (e). **(g)** Time course of cAMP production following light stimulation of OptoXRs (λ=480 ± 7.5 nm, I=1.97 mW/cm^2, 40 s, 4000 fl). **(h)** Maximal cAMP signals elicited by OptoXRs (see (f) for light stimulation parameters). For f-h: n=9, 3 independent experiments. Data shown as mean ± S.E.M.
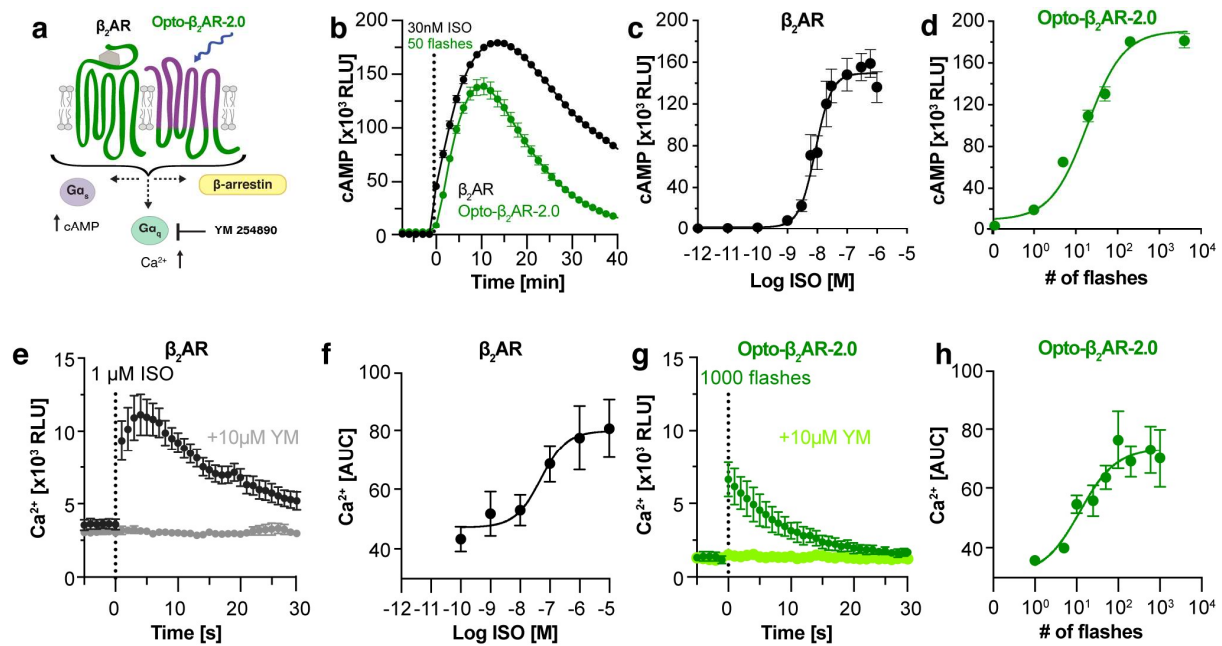
Fig. 3: Signaling by Opto-β₂AR-2.0. (a) Signaling pathways examined for β₂AR and Opto-β₂AR-2.0. **(b)** Time course of cAMP production following stimulation of β₂AR with ISO (1 μM) or Opto-β₂AR-2.0 with light (λ=480 ± 7.5 nm, I=1.97 mW/cm², 0.5 s, 50 fl). **(c, d)** Dose-dependent cAMP production following stimulation of β₂AR with ISO or Opto-β₂AR-2.0 with light (λ=480 ± 7.5 nm, I=1.97 mW/cm², 0.01-20 s, 1-2000 fl). **(e, g)** Time course of intracellular Ca²⁺ mobilization following stimulation of β₂AR with ISO (as in b) or Opto-β₂AR-2.0 with light (as in b). Signaling was abolished by the Gα_q inhibitor YM. **(f, h)** Dose-dependent Ca²⁺ mobilization following stimulation of β₂AR with ISO or Opto-β₂AR-2.0 with light (λ=480 ± 7.5 nm, I=1.97 mW/cm², 0.1-10 s, 1-1000 fl). For c, d, f, h: n=9-12, 3-4 independent experiments. Data shown as mean ± S.E.M.
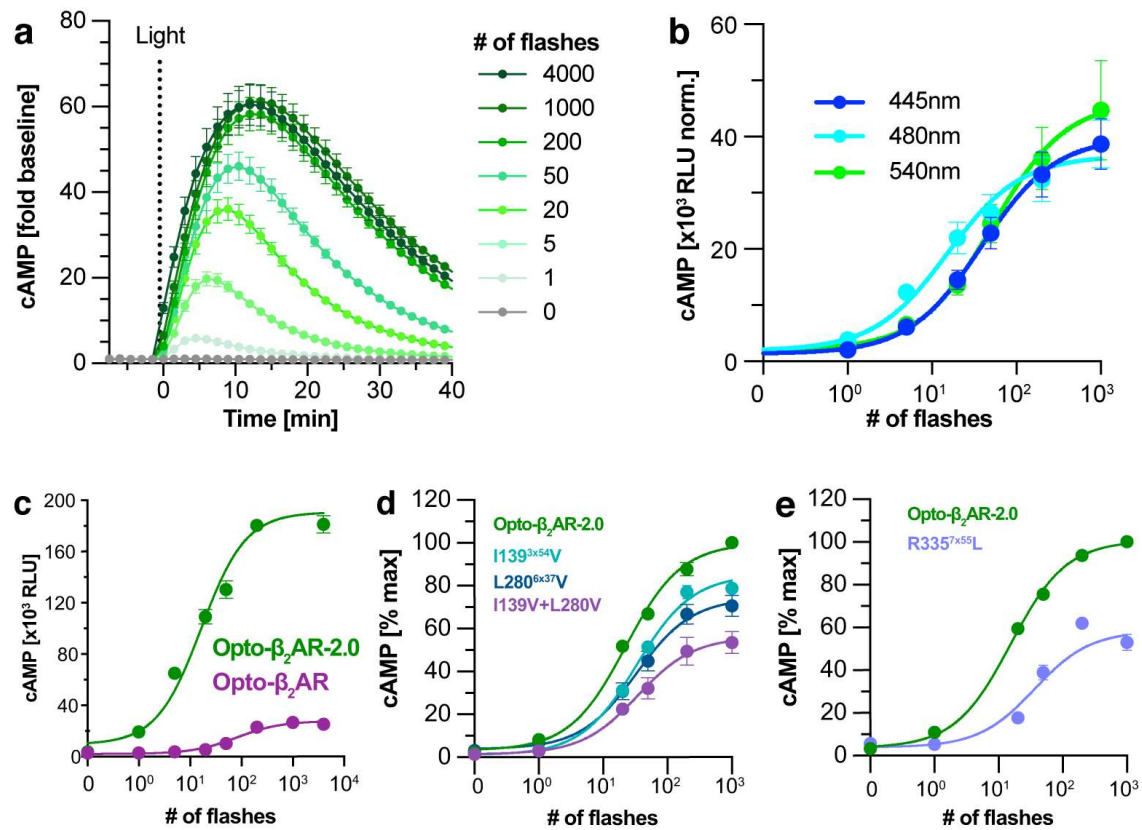
24

Fig. 4: Optical activation of Opto-β₂AR-2.0, Opto-β₂AR and variant receptors . (a) Time course of cAMP production following stimulation of Opto-β₂AR-2.0 (λ=480 ± 7.5 nm, I=1.97 mW/cm^2, 0.01-40 s, 1-4000 fl). **(b)** Stimulation of Opto-β₂AR-2.0 with light of different wavelengths (λ=480 ± 7.5 nm, I=1.97 mW/cm^2; λ=445 ± 7.5 nm, I=1.75 mW/cm^2; λ=540 ± 7.5 nm, I=1.35 mW/cm^2; for all wavelengths: 0.01-10 s, 1-1000 fl). **(c)** Stimulation of Opto-β₂AR and Opto-β₂AR-2.0 with increasing light doses (λ=480 ± 7.5 nm, I=1.97 mW/cm^2, 0.01-40 s, 1-4000 fl). **(d, e)** Stimulation of Opto-β₂AR-2.0 reversal variants I139^{3x54}V, L270^{6x37}V and the corresponding double mutant (d) as well as R335^{7x55} (e) with light (λ=480 ± 7.5 nm, I=1.97 mW/cm^2, 0.01-10 s, 1-1000 fl). For b-e: n=6-9, 2-3 independent experiments. Data shown as mean ± S.E.M.
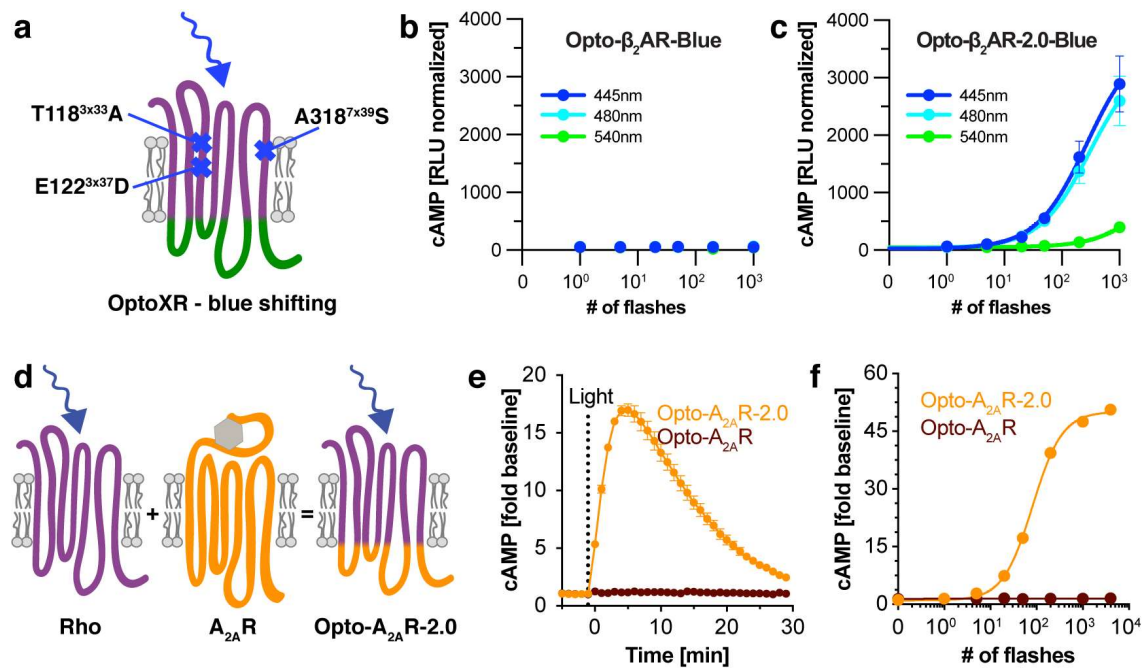
25

Fig. 5: Diversified receptor variants. (a) Substitutions in Opto-β_2AR and Opto-β_2AR-2.0 to engineer variants termed Opto-β_2AR-Blue and Opto-β_2AR-2.0-Blue. **(b,c)** Stimulation of Opto-β_2AR-Blue and Opto-β_2AR-2.0-Blue with light of different wavelengths (λ=480 ± 7.5 nm, I=1.97 mW/cm^2; λ=445 ± 7.5 nm, I=1.75 mW/cm^2; λ=540 ± 7.5 nm, I=1.35 mW/cm^2; for all wavelengths: 0.01-10 s, 1-1000 fl). **(d)** Opto-A_{2A}R-2.0. **(e)** Time course of cAMP production following stimulation of Opto-A_{2A}R and Opto-A_{2A}R-2.0 with light (λ=480 ± 7.5 nm, I=1.97 mW/cm^2, 0.5 s, 50 fl). **(f)** Dose-dependent cAMP production following stimulation Opto-A_{2A}R-2.0 and Opto-A_{2A}R with light (λ=480 ± 7.5 nm, I=1.97 mW/cm^2, 0.1-20 s, 1-2000 fl). For panels b, c, f: n=6-9, 2-3 independent experiments. Data shown as mean ± S.E.M.